Modern Physics Letters B
Vol. 38, No. 13 (2024) 2450091 (19 pages)

DOI: 10.1142/S021798492450091X

World Scientific
www.worldscientific.com

# Anti-resonance fiber propagating 86 orbital angular momentum modes with high purity for a long distance

Yutong Liu*, Wei Liu*, Jingwei Lv*, Jianxin Wang*, Lin Yang*, Qiang Liu*, Paul K. Chu† and Chao Liu*,‡

*School of Physics and Electronic Engineering,
Northeast Petroleum University,
Daqing 163318, China

†Department of Physics,
Department of Materials Science and Engineering,
and Department of Biomedical Engineering,
City University of Hong Kong,
Tat Chee Avenue, Kowloon, Hong Kong, China
‡msm-liu@126.com

Received 3 July 2023
Revised 5 August 2023
Accepted 11 September 2023
Published 3 November 2023

Future advances in information transmission technology require better capacities for fiber optics communication. As a new degree of freedom, the orbital angular momentum (OAM) has attracted extensive attention in the field of mode division multiplexing. Herein, an anti-resonance fiber (ARF) is designed with three different materials, SF11, LaSF09, and $SiO_2$, for the negative curvature tube. Systematic analysis and optimization are carried out to determine the number of layers of the negative curvature tubes in the cladding, the number of second-layer cladding tubes, and thickness of the annular area. The finite element analysis software COMSOL is utilized to calculate the effective refractive index difference, dispersion, limiting loss, and other characteristics. The ARF can stably transmit 86 OAM modes in the wavelength range between 1.2 and 2.0 $\mu$m, and the minimum refractive index difference is greater than $1 \times 10^{-4}$, which effectively reduces the mode abridgment. The nonlinear coefficients of the $HE_{23,1}$ mode and the OAM purity of $HE_{1,1}$ mode are $0.34\,km^{-1} \cdot W^{-1}$ and 99.43%, respectively, thus facilitating stable transmission of OAM modes for a long transmission distance. The anti-resonance fiber has significant application potential in long-distance network information transmission, relay communication, and other communication areas.

*Keywords*: Orbital angular momentum (OAM); anti-resonance fiber (ARF); fiber optics communication; mode purity.

## 1. Introduction

With the continuous development of 6G technology and big data technology, the requirements for information transmission and communication capacity are

‡Corresponding author.

becoming increasingly high. Traditional communication methods include wireless communication, electrical communication, and fiber optics communication.[1] With recent advancements in modern communication, some new technologies have emerged, such as efficient solar absorbers arranged using multi-layer nanodisks, and the design of solar cells using inorganic[2–4] and organic powder doping.[5–7] At the same time, fiber optics communication has become the pillar of the communication industry. However, when the traditional single-mode optical fiber is used in communication, it can no longer break the Shannon–Hartley theorem, and therefore, finding a more suitable degree of freedom for fiber optics communication is becoming increasingly significant. The main methods of fiber optics communication include wavelength division multiplexing,[8] time division multiplexing,[9] partial division multiplexing,[10] and so on. However, it is still difficult to increase the communication capacity and a better multiplexing method is highly desirable.

Multiplexing is a method of combining several independent signals into a composite signal that can be transmitted simultaneously in the same channel.[11] That is, multiplexing techniques provide shared channels. In order to solve the problem of communication capacity, module division multiplexing (MDM)[12] and space division multiplexing (SDM)[13] have been adopted by ultra-large capacity transmission links due to their higher scalability, high accuracy and efficiency, low complexity, fast computing speed, and reusability. Nevertheless, traditional multiplexing methods mainly rely on frequencies, wavelengths, and phases and cannot achieve stable transmission with an ultra large capacity. The orbital angular momentum existing in the vortex carries the spiral phase factor.[14] There are infinite orthogonal bases, if the information to be transmitted can be loaded into these orthogonal bases. Theoretically, extremely high capacity can be achieved in fiber optics communication.[15] Compared to traditional communication methods, it increases the capacity and distance of photons transmitted in the optical fibers.

Common optical fibers for communication include single-mode fibers,[16] multimode fibers,[17] and photonic crystal fibers (PCF)[18,19] and high-capacity photonic crystal fiber devices have been proposed. For instance, Yue *et al.*[20] have designed a PCF with hexagonal cladding pores with $As_2S_3$ and two OAM modes due to the large refractive index difference between the materials. Huang *et al.*[21] have proposed a dispersion-flat PCF with a minimum variation of 10 ps/(km.nm) that can transmit 30 OAM modes and Ma *et al.*[22] have designed a PCF that transfers 180 OAM modes at 1.5–1.7 $\mu$m. However, owing to the easy occurrence of mode coupling in the transmission of OAM modes in photonic crystal fibers, it is difficult to minimize losses. In addition, the manufacturing process is complex and there is uneven dispersion. As a consequence, a more suitable carrier for OAM communication is highly desirable.[23]

The anti-resonance fiber (ARF)[24] is formed by arranging negative curvature antiresonant tubes in a certain way. The special light guiding mechanism makes it a simpler preparation technology with a smaller limiting loss and longer communication distance compared to PCF. If OAM is loaded into the ARF, the communication

efficiency[25] can be improved. Md *et al.*[26] have proposed an ARF that supports 64 OAM modes with a bandwidth of 400 nm and good transmission range. Chen *et al.*[27] have proposed a negative curvature ARF with good single mode characteristics and losses less than 1 dB/km and Chaudhuri *et al.*[28] have designed an ARF model with a nested elliptical cladding layer with low losses at 1.55 $\mu$m. However, in spite of recent advances, there are still few high-capacity communication devices based on ARF for OAM.

Herein, the COMSOL Multiphysics software is implemented to design and simulate an ARF that can support the transmission of 86 OAM modes. The parameters that affect the transmission of OAM modes are analyzed, including the effective refractive index difference, dispersion, mode purity, dispersion, mode field area, and other factors in the wavelength range of 1.2–2.0 $\mu$m. Our results disclose that the minimum nonlinear coefficient is $0.37\,\mathrm{km^{-1}\cdot W^{-1}}$, least dispersion change is only $4.81\,\mathrm{ps/(km\cdot nm)}$, mode purity is greater than 96.17%, and effective refractive index difference is greater than $1\times10^{-4}$. Furthermore, optical confinement increases by using a triple anti-resonant glass tube, which also ensures the stability and less losses in OAM mode transmission.

## 2. ARF Design and Basic Theory

The angular momentum[29] is divided into the spin angular momentum and orbital angular momentum. The orbital angular momentum mainly exists in the vortex beam with a spiral phase. Owing to the orthogonality of the OAM beams with different topological charges, the theoretical number of topological charges of OAM beams can be any integer, and multiple OAM beams[30] with different topological charges can be used as carriers for information transmission.

The OAM mode is formed by the superposition of the odd and even components of the HE mode or EH mode as shown in Eq. (1)[31]:

$$\begin{aligned}\mathrm{OAM}^{\pm}_{\pm l,m} &= \mathrm{HE}^{\mathrm{even}}_{l+1,m} \pm i\mathrm{HE}^{\mathrm{odd}}_{l+1,m} \quad \text{and}\\ \mathrm{OAM}^{\mp}_{\pm l,m} &= \mathrm{EH}^{\mathrm{even}}_{l-1,m} \pm i\mathrm{EH}^{\mathrm{odd}}_{l-1,m},\end{aligned} \tag{1}$$

where $\boldsymbol{l}$ is the topological charge number, $m$ is the radial order usually equal to 1. HE and EH represent the mixed modes of light waves, while even and odd stand for the even and odd modes, respectively. The positive and negative signs in the OAM superscript show the direction of circular polarization. "+" represents right-handed circular polarization and "−" represents left-handed circular polarization.[32] When $\boldsymbol{l}=1$, the OAM mode has the same polarization mode and rotation direction and can only serve as two channels. When $\boldsymbol{l}\geq 2$, the OAM modes have the same and opposite polarization modes, which can serve as four independent channels. Therefore, the number of OAM modes that can be transmitted in the fiber is $4\times\boldsymbol{l}-2$. The positive and negative signs before $\boldsymbol{l}$ represent the rotation direction of the wave-front phase, and the transmission constants between the intrinsic modes of the linearly

superimposed OAM mode[33] are the same. By performing finite element simulation based on COMSOL, the light field distribution of the HE mode and EH mode can be obtained.

In order to improve the transmission efficiency of the OAM mode, an ARF consisting of multiple negative curvature anti-resonance tubes with different diameters is designed and the cross-section and 3D schematic diagram are shown in Figs. 1(a) and 1(b).

There is a layer of 25 negative curvature glass tubes with a smaller diameter tangent to the annular region as well as two layers of anti-resonant tubes with different diameters tangent outside the circular area. The first layer is composed of 31 anti-resonance negative curvature tubes filled with SF11 glass with a high refractive index forming the refractive index difference with the annular region and allowing for rapid photon transmission. The second layer comprises 24 anti-resonant negative curvature tubes made of $SiO_2$. The thickness of the two layers of the glass tubes is the same in order to better constrain the photons. The annular area consists of a large negative curvature glass tube with a thickness of $\boldsymbol{t}_1$ made of LaSF09. Since LaSF09 has a minimum refractive index of 1.8164 in the 1.2–2.0 $\mu$m band, the cladding tube has a refracture index of 1.4381 that will increase the effective refractive index difference and stabilize the transmission of the OAM mode. The refractive indexes of the materials are determined by the Sellmeier Equation shown below[34]:

$$n^2(\lambda) = 1 + \frac{A_1\lambda^2}{\lambda^2 - B_1} + \frac{A_2\lambda^2}{\lambda^2 - B_2} + \frac{A_3\lambda^2}{\lambda^2 - B_3}. \tag{2}$$

Table 1 shows the parameters of different materials.

The light blue area represents the $SiO_2$ cladding of the optical fiber. The inner radius of the circular area is $\boldsymbol{R_1}$ and the thickness is $\boldsymbol{t_1}$. The diameter of the inner negative curvature tube is $\boldsymbol{d_1}$, the diameters of the two outer negative curvature

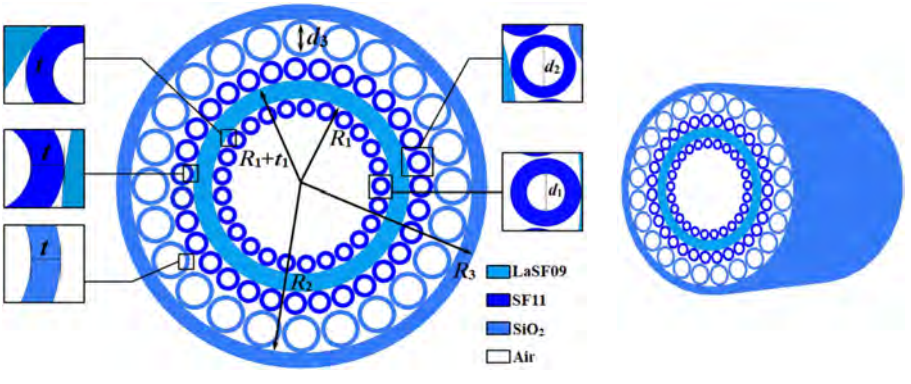


(a) (b)

Fig. 1. (Color online) (a) Cross-section and (b) 3D schematic diagram of the ARF.

Table 1. Parameters of different materials.

| | Parameters | | | | | |
|---|---|---|---|---|---|---|
| Material | $A_1$ | $A_2$ | $A_3$ | $B_1$ | $B_2$ | $B_3$ |
| LaSF09 | 2.00029547 | 0.298926886 | 1.80691843 | 0.0121426017 | 0.0538736236 | 156.530829 |
| SF11 | 1.73759695 | 0.313747346 | 1.89878101 | 0.013188707 | 0.0623068142 | 155.23629 |
| $SiO_2$ | 0.6961663 | 0.4079426 | 0.897479 | 0.0684043 | 0.1162414 | 9.896161 |

tubes are $\boldsymbol{d_2}$ and $\boldsymbol{d_3}$, respectively, and the wall thickness is $\boldsymbol{t}$. The radius of the cladding is $\boldsymbol{R_2}$. In order to improve the transmission and communication characteristics of OAM, the number of layers of the negative curvature tubes in the cladding, the number of second layer cladding tubes, and the thickness of the annular area are optimized.

Figures 2(a) and 2(b) show the optimized number of cladding anti-resonance tube layers based on the mode field area at 1.55 $\mu$m. Without changing the radius of the annular region and the number of anti-resonance tubes, there are 31 anti-resonance glass tubes near the annular region. When the anti-resonance tube has only one layer, the mode field areas are 107.97 $\mu m^2$ and 147.57 $\mu m^2$ for the $HE_{1,1}$ mode and $HE_{23,1}$ mode, respectively. If the number of layers of the anti-resonance tube is 2, the mode areas of the $HE_{1,1}$ mode and $HE_{23,1}$ mode are 109.85 $\mu m^2$ and 154.70 $\mu m^2$, respectively.

Taking the number of layers of the cladding anti-resonance tube to be 2, the thickness of the annular LaSF09 area is optimized based on the number of transportable OAM modes as shown in Fig. 3. When $\boldsymbol{t_1} < 1.5\,\mu$m, a large amount of the photon energy leaks into the cladding. If the gauge of the annular region is greater than 2.5 $\mu$m, the electric field distributions of the HE and EH modes are distorted.

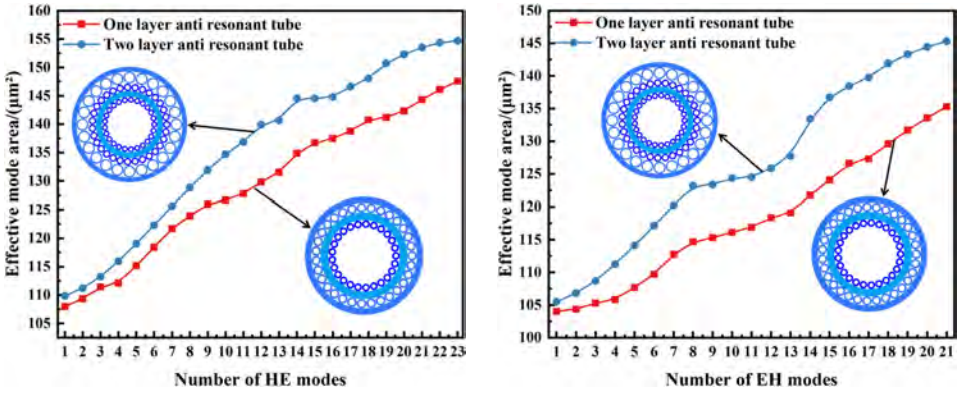


(a) (b)

Fig. 2. (Color online) (a) and (b) Mode field areas for different layers of the anti-resonant tubes.

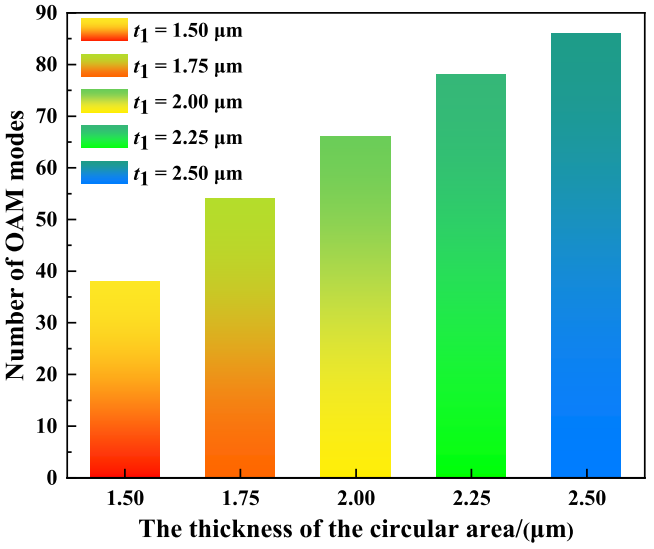


Fig. 3. (Color online) Numbers of OAM modes for different thicknesses of the circular region.

Consequently, information transmission is hindered and so the range of $\boldsymbol{t_1}$ is $1.5\,\mu\text{m} < \boldsymbol{t_1} < 2.5\,\mu\text{m}$. As $\boldsymbol{t_1}$ increases, the number of OAM modes goes up. When the thickness of the annular area is $2.5\,\mu$m, there is a maximum number of OAM modes of 86 that can be transmitted in the ARF. Therefore, the optimal $\boldsymbol{t_1}$ is $2.5\,\mu$m.

When the numbers of layers of the cladding tube and $\boldsymbol{t_1}$ are 2 and $2.5\,\mu$m, respectively, based on the mode purity, the number of second layer anti-resonance tubes is optimized at a wavelength of $1.55\,\mu$m. If the number of the anti-resonant tubes is 32 and the negative curvature tubes intersect, the structural design principle is not satisfied. When the number of glass tubes is less than 16, light cannot be confined in the annular region resulting in significant losses. Therefore, the number of the second layer of the resonance tubes is between 16 and 31. Figures 4(a) and 4(b) show that when the number of anti-resonance tubes is 20–28, the mode purity is inversely proportional to the number, but if the number of inverse resonant tubes is outside this range, it is proportional to the number. When the number of the anti-resonant tubes is 31, the purities of the HE and EH modes are the highest reaching 98.92% and 98.50%, respectively. In summary, the number of cladding anti-resonance tubes is 2, the number of second layer inverse resonant tubes is 31, and the thickness of the annular region $\boldsymbol{t_1}$ is $2.5\,\mu$m.

This structure can be manufactured through stacking and stretching techniques.[35] Stack multiple negative curvature tubes with different radii and the same thickness on the inner and outer surfaces of a circular area with a central longitudinal axis, so that they are spaced around the inner and outer surfaces, and then wrap a circle of larger negative curvature tubes around their periphery, so that the two layers of tube walls come into contact. When the distance from the negative

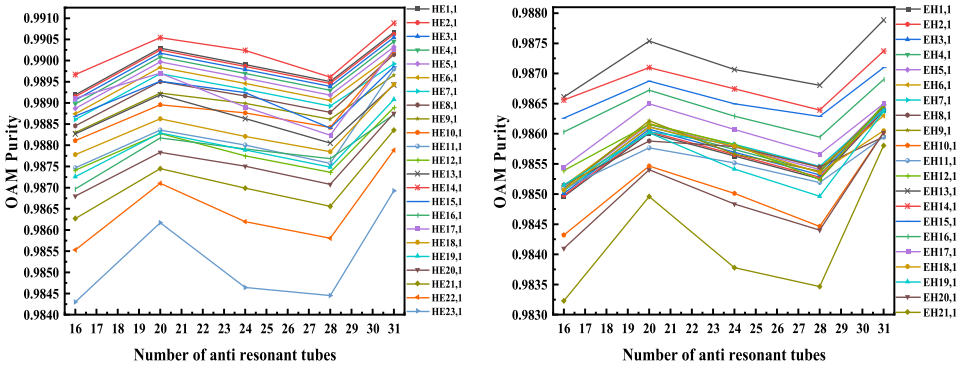


(a) (b)

Fig. 4. (Color online) (a) and (b) OAM purity for different numbers of second layers of the anti-resonant tubes.

curvature tube to the central vertical axis is greater than the distance between the central longitudinal axis of the negative curvature tube and the central direct-axis, fiber drawing can be carried out.

## 3. Results and Discussion

### 3.1. *Transmitted modes*

The intrinsic modes of the OAM mode in optical fibers are $HE_{l+1,m}$ and $EH_{l-1,m}$. For the electromagnetic mixed modes of the same order, the HE and EH modes generate a phase difference of $\pi/2$.[36] Figures 5(a)–5(f) show that the electric field distributions in the $z$-direction for some HE and EH modes at a wavelength of 1.55 $\mu$m. The HE mode is closer to the cladding, while the EH mode is near the fiber core. As the topological charge continues to increase, the trend of photons leaking into the cladding increases.[37] The highest order HE and EH modes are $HE_{23,1}$ and $EH_{21,1}$, and the ARF can support up to the 22nd order OAM mode transmission, namely $OAM_{22,1}$. Therefore, a maximum of $22 \times 4 - 2 = 86$ OAM modes can be supported for transmission at 1.2–2.0 $\mu$m. Figures 5(g)–5(i) show the phase distributions of the OAM modes, although the phase distribution changes with the topological charge number, the energy of the optical field is well bound within the ring core, and the structure of the OAM mode is always helical, with no phase distortion. When the topological charge number is $n$, the phase change of OAM mode is always $2n\pi$, which can be demultiplexed by the conjugate phase mode.[38]

### 3.2. *Effective refractive index and refractive index difference*

In OAM fiber optics communication, the effective refractive index is the physical quantity to analyze the dispersion as well as the effective refractive index difference. When transmitting optical signals using optical fibers as a medium, the wave number

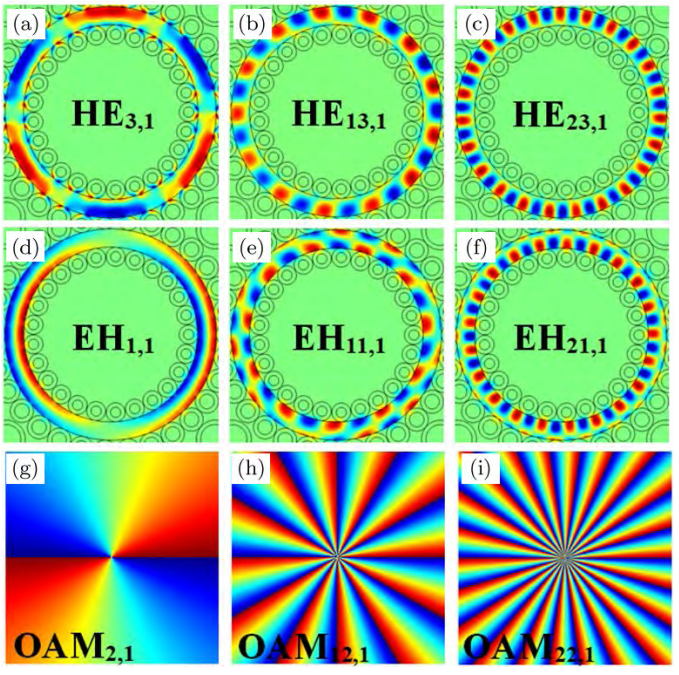


Fig. 5. (Color online) (a)–(f) Optical field profiles in the z orientation of the HE and EH modes and (g)–(i) Phase diagrams of the partially indicated OAM modes.

will be higher than in vacuum.[39] Figures 6(a) and 6(b) show the negative wavelength-dependent trend of the effective refractive indexes of the HE and EH modes in the wavelength range of 1.2–2.0 $\mu$m. The larger the wavelength, the bigger is the first derivative of the refractive index. Additionally, the changes in the high-order modes are substantial, while the variations in the low-order modes are relatively small.

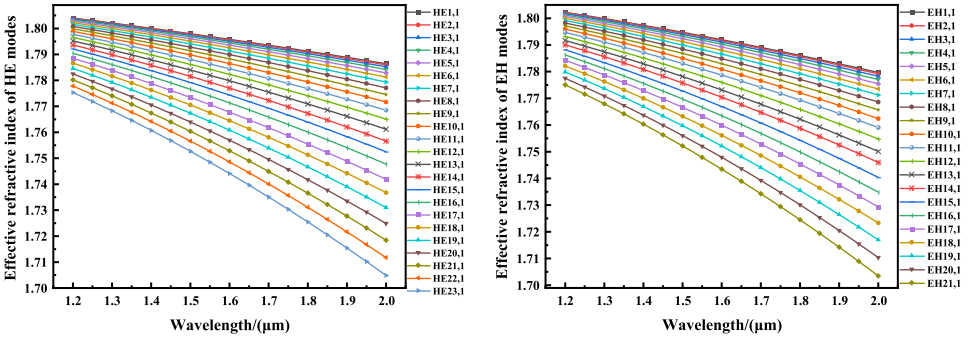


(a) (b)

Fig. 6. (Color online) (a) and (b) Effective refractive indexes of the HE modes and EH modes.

This is because as the wavelength increases, the light field energy diffuses gradually from the fiber core to the cladding.[40]

The effective transmission of OAM mode in optical fibers depends on whether the effective refractive index difference between the HE mode and EH mode is greater than $1 \times 10^{-4}$. Figure 7 shows the relationship of the differences between each group of $HE_{l+1,m}$ and $EH_{l-1,m}$ as a function of wavelength. The change in the effective refractive index difference is proportional to the wavelength. When the wavelength is $1.2\,\mu$m, $OAM_{22,1}$ has the minimum effective refractive index difference of $2.64 \times 10^{-4}$, which is greater than $1 \times 10^{-4}$. When the wavelength is $1.55\,\mu$m, the vast majority of the OAM modes reach the order of magnitude of $10^{-3}$, and the maximum is $2.84 \times 10^{-3}$ for the $OAM_{2,1}$ mode. The higher the effective refractive index difference, the greater is the transmission efficiency of OAM mode, thus reducing the probability of coupling the LP mode[41] between the two modes to ensure the transmission quality.

### 3.3. *Chromatic dispersion*

Fiber dispersion[42] refers to the phenomenon of optical pulse broadening in an optical fiber caused by different group velocities at different frequencies in the spectral components of the light source. The smaller the dispersion in the fiber and the flatter the dispersion at a certain wavelength, the better is the performance of the fiber and the more effective the OAM transmission. The dispersion consists of material dispersion and waveguide dispersion.[43] The dispersion of LaSF09-doped annular region

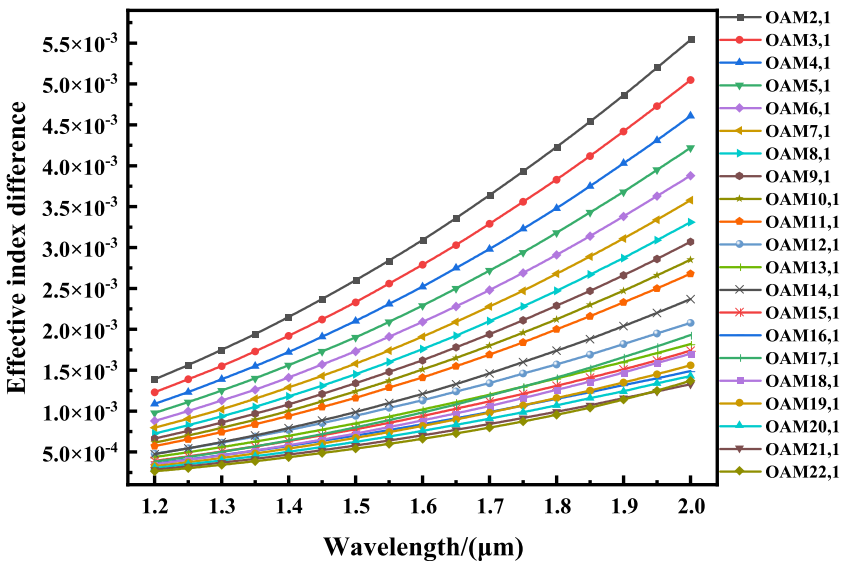


Fig. 7. (Color online) Effective index difference of the OAM modes.

of the glass tube can be obtained by Eq. (2) and shown in Table 1. When $\lambda$ is in the range of 1.2–2.0 $\mu$m, the refractive index of LaSF09 is 1.8166–1.8164. The waveguide dispersion dominates, and the total dispersion can be obtained from the relationship between the wavelength and effective refractive index as shown in Eq. (3)[44]:

$$D = -\frac{\lambda}{c}\frac{d^2\mathrm{Re}(n_{\mathrm{eff}})}{d\lambda^2}, \tag{3}$$

where $c$ is the speed of light ($3 \times 10^8$ m/s) and $\mathrm{Re}(n_{\mathrm{eff}})$ is the real part of the effective refractive index. Figure 8 shows that the dispersion of the OAM modes is proportional to the wavelength between 1.2 $\mu$m and 2.0 $\mu$m. For the same wavelength, the higher the order of the modes of HE and EH, the greater is the dispersion due to the instability of the higher order modes during transmission and easy leakage to the cladding.[45] When the wavelength is 1.2 $\mu$m, the minimum dispersion is 59.45 ps/(km · nm) for the EH mode and 38.03 ps/(km · nm) for the HE mode. When the wavelength is 2.0 $\mu$m, the minimum dispersion is 347.08 ps/(km · nm) for the EH mode and 320.76 ps/(km · nm) for the HE mode. The HE mode is closer to the cladding area of the fiber, while the EH mode is closer to the fiber core, making it more susceptible to the influence of external air. Hence, the dispersion of the HE mode is smaller than that of the EH mode. The dispersion variation of the lower-order modes in the figures is quite smooth, especially the $\mathrm{HE}_{1,1}$ mode showing only 4.81 ps/(km · nm). The structure described in this paper possesses a relatively good flat dispersion boding well for fast transmission of information in the optical fibers.

### 3.4. *Effective mode area and nonlinear coefficients*

The effective mode field area[46] quantitatively measures the transverse area occupied by a certain mode in a waveguide or fiber. It reflects the quality of the OAM mode

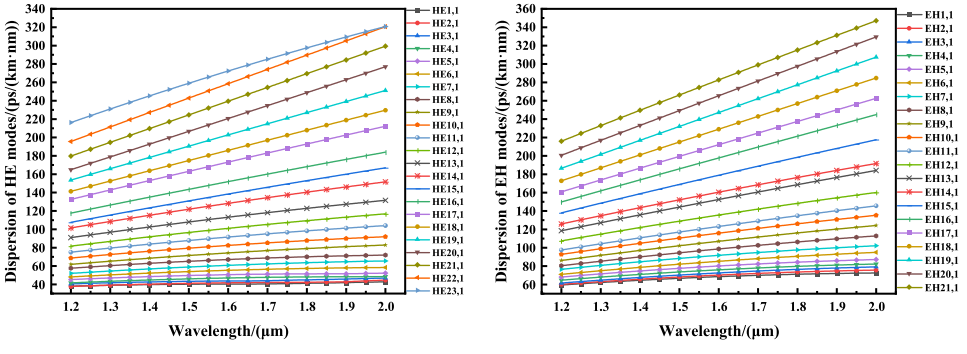


(a) (b)

Fig. 8. (Color online) (a) and (b) Dispersions of the HE and EH modes.

transmission in the optical fibers. The effective mode area shows a positive correlation with wavelength and the order of the OAM mode. The reason for the larger effective mode field area of higher-order modes is that as the wavelength increases, the limiting ability of the fiber's energy concentration area to light[47] weakens, leading to diffusion to the cladding. The effective mode area is determined by Eq. (4)[48]:

$$A_{\text{eff}} = \frac{\left(\int\int |E(x,y)|^2 dxdy\right)^2}{\int\int |E(x,y)|^4 dxdy}. \tag{4}$$

The effective mode areas of the HE and EH modes are shown in Figs. 9(a) and 9(b), which indicates that the mode areas of the HE and EH modes are proportional to the wavelength in the range of 1.2–2.0 $\mu$m. The larger the number of modes, the larger is the area of the mode field. The maximum mode field area of the $HE_{23,1}$ mode is 162.78 $\mu m^2$, and that of the $EH_{21,1}$ mode is 150.46 $\mu m^2$. At a wavelength of 1.55 $\mu$m, the effective mode area of the $HE_{1,1}$ mode is the smallest at 109.85 $\mu m^2$, and that of the $HE_{23,1}$ mode is the largest at 154.70 $\mu m^2$. The effective mode area of the HE mode is larger than that of the EH mode allowing it to carry more photon energy.

The nonlinear effect[49] refers to the influence caused by the nonlinear polarization of the medium under the action of strong light. The nonlinear coefficient which also measures the nonlinear effects in the fiber is inversely proportional to the mode area. A smaller nonlinear coefficient[50] translates into a weaker nonlinear effect in the fiber, and a stronger one vice versa. Smaller nonlinear effects are more favorable to anti-resonance fiber transmission of the OAM mode. It is calculated by Eq. (5)[51]:

$$\gamma = \frac{2\pi n_2}{\lambda A_{\text{eff}}}, \tag{5}$$

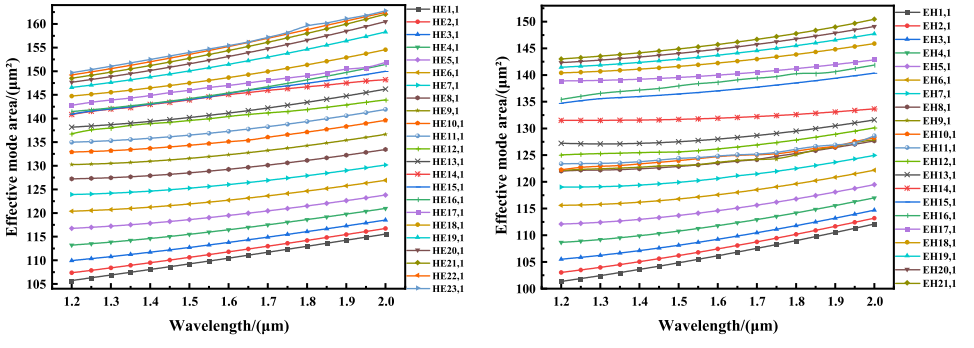


(a) (b)

Fig. 9. (Color online) (a) and (b) Effective mode areas of the HE and EH modes.

where $\lambda$ is the wavelength, $A_{\text{eff}}$ is the effective mode area, and $n_2$[52] is the nonlinear refractive index coefficient of LaSF09. The variations of the nonlinear coefficients of the HE and EH modes are shown in Figs. 10(a) and 10(b).

Figure 10 shows that the nonlinear coefficients of the HE and EH modes decrease gradually with increasing wavelength in the wavelength range of 1.2–2.0 $\mu$m, and the nonlinear coefficient of HE mode is lower than that of EH mode. At a wavelength of 1.55 $\mu$m, the nonlinear coefficient is the smallest at 0.44 $\text{km}^{-1} \cdot \text{W}^{-1}$ for the $\text{HE}_{23,1}$ mode and largest at 0.62 $\text{km}^{-1} \cdot \text{W}^{-1}$ for the $\text{HE}_{1,1}$ mode. The nonlinear coefficients of the transmittable OAM modes in the optical fibers are all between 0.34 km–0.87 $\text{km}^{-1} \cdot \text{W}^{-1}$ at wavelengths between 1.2 $\mu$m and 2.0 $\mu$m. Therefore, there is a small nonlinear effect in this fiber making the OAM mode less distorted during transmission.

### 3.5. *Numerical aperture*

The numerical aperture (NA)[53] of the optical fiber is an important parameter of the ARF. The NA takes into account the ability of the fiber to receive light and effects on mode dispersion. The NA is mainly related to the refractive index of the core and the refractive index difference between the core and cladding. The relationship with wavelength is expressed by Eq. (6)[54]:

$$\text{NA} = \left(1 + \frac{\pi A_{\text{eff}}}{\lambda^2}\right)^{-\frac{1}{2}}, \tag{6}$$

where $\lambda$ is the wavelength and $A_{\text{eff}}$ is the effective mode area. The value of NA is inversely proportional to the area of the mode field. The variations of the numerical apertures of the HE and EH modes are shown in Figs. 11(a) and 11(b).

In the wavelength range of 1.2–2.0 $\mu$m, the trend of NA is positively correlated with the wavelength and the NA of the EH mode is larger than that of HE mode.

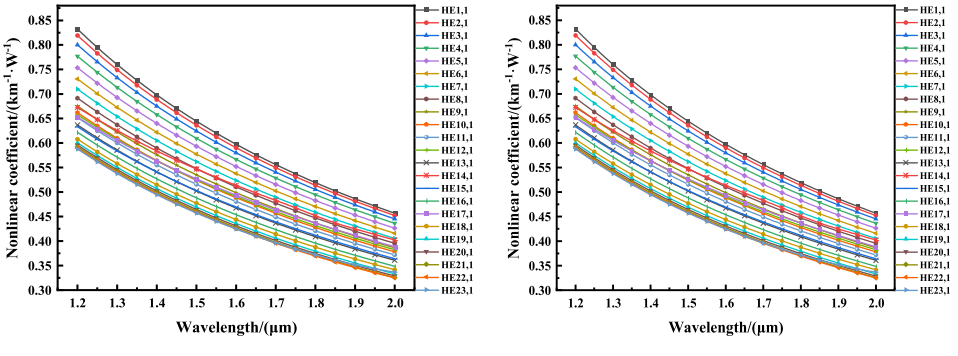


(a) (b)

Fig. 10. (Color online) (a) and (b) Nonlinear coefficients of the HE and EH modes.

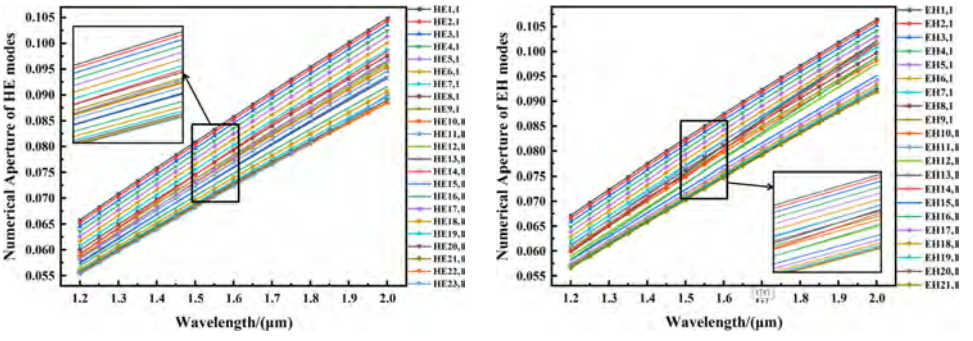


(a) (b)

Fig. 11. (Color online) (a) and (b) Numerical apertures of the HE mode and EH mode.

The maximum NA of the $HE_{23,1}$ mode is 0.900 and that of the $EH_{21,1}$ mode is 0.919. The maximum NA at 1.55 $\mu$m is 0.833 for the $HE_{1,1}$ mode, and the NA for this band is in the range of 0.070–0.084. The larger the NA, the stronger is light reception leading to good transmission effects.

### 3.6. *Confinement losses*

When the OAM modes are transmitted through the ARF, because of the different number of glass tubes in the fiber, some modes may leak out of the cladding to produce losses. The limiting loss[55] reflects the good or bad performance of the fiber. The lower the loss, the better is the performance of the fiber, and the longer the distance over which the OAM mode can be transmitted. The limiting loss can be obtained by Eq. (7)[56,57]

$$L = \frac{2\pi}{\lambda} \frac{20}{\ln(10)} 10^6 \mathrm{Im}(n_{\mathrm{eff}}), \tag{7}$$

where $\lambda$ is the wavelength and $\mathrm{Im}(n_{\mathrm{eff}})$ is the imaginary part of the effective refractive index. Figures 12(a) and 12(b) show the limiting losses of the HE and EH modes at a wavelength of 1.55 $\mu$m.

There is no certain regularity in the limiting losses of the HE and EH modes, but the losses are between $10^{-10}$ dB/m and $10^{-8}$ dB/m. Table 2 illustrates that the light is transmitted in the ARF with less losses and can also be transmitted in a steady state.

### 3.7. *Mode purity*

The mode purity[58] characterizes the quality of the OAM modes. The higher the mode purity, the more stable is transmission of the OAM mode. The mode purity is mainly related to the electric field modes in the ring region and cross-section of the fiber as

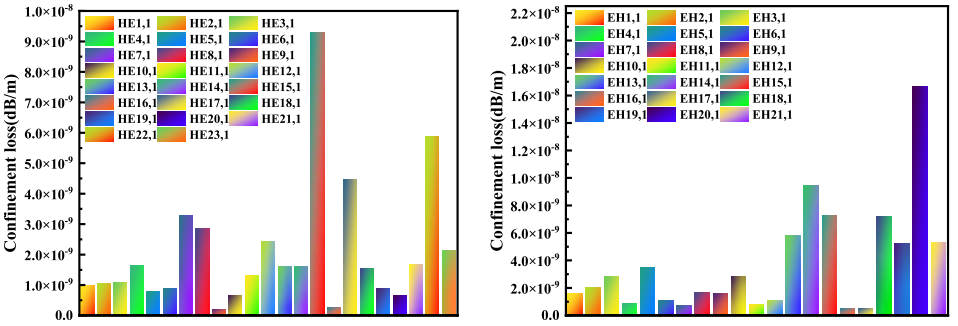


(a) (b)

Fig. 12. (Color online) (a) and (b) Confinement losses of the HE and EH modes at 1.55 $\mu$m.

Table 2. Confinement losses for different HE and EH modes.

| Models | $HE_{1,1}$ | $HE_{8,1}$ | $HE_{15,1}$ | $HE_{23,1}$ |
|---|---|---|---|---|
| Confinement loss/(dB/m) | $9.68 \times 10^{-10}$ | $2.86 \times 10^{-9}$ | $9.3 \times 10^{-9}$ | $2.13 \times 10^{-9}$ |
| | $EH_{1,1}$ | $EH_{8,1}$ | $EH_{15,1}$ | $EH_{21,1}$ |
| Confinement loss/(dB/m) | $1.52 \times 10^{-9}$ | $1.65 \times 10^{-9}$ | $7.2 \times 10^{-9}$ | $5.26 \times 10^{-9}$ |

shown by Eq. (8)[59]:

$$\eta = \frac{I_r}{I_c} = \frac{\int\int_{\text{ring}} |\vec{E}|^2 dxdy}{\int\int_{\text{cross-section}} |\vec{E}|^2 dxdy}, \tag{8}$$

where $I_r$ is the high refractive index negative curvature tube in the annular region and $I_c$ is the average electric field intensity across the ARF cross-section, both of which can be calculated by COMSOL. The variation of the mode purity between the HE and EH modes is shown in Figs. 13(a) and 13(b).

In the wavelength range of 1.2–2.0 $\mu$m, the mode purity decreases gradually with increasing wavelength, and there is a regular and gradual decrease. The mode purity of both the HE and EH modes is greater than 96.17% which is high. At the wavelength of 1.55 $\mu$m, the maximum mode purity of the HE mode is 98.92% and the maximum mode purity of the EH mode is 98.50%. The OAM mode offers significant mode purity and makes transmission more stable.

### 3.8. *Walk-off length*

The transmission speeds of the odd and even modes of the same order OAM mode in the fiber are different, which may cause walk-off effects and make it impossible for the odd and even modes of the intrinsic mode to synthesize OAM modes. The walk-away length[60] can be used to measure the maximum transmission distance of the mode

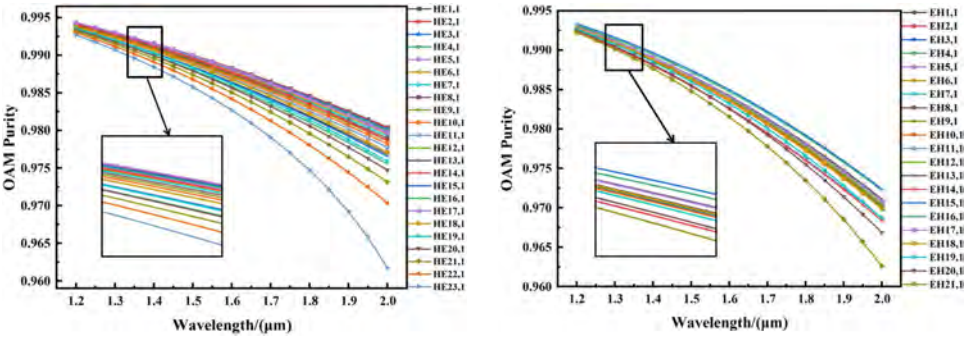


(a) (b)

Fig. 13. (Color online) (a) and (b) OAM purity of the HE and EH modes.

before the walk-off effect occurs. The walk-away length is proportional to the transmission distance in the fiber as shown by Eq. (9)[61]:

$$L_{10\,\mathrm{ps}} = \frac{c \times 10\,\mathrm{ps}}{n_{\mathrm{eff}}^{\mathrm{even}} - n_{\mathrm{eff}}^{\mathrm{odd}}} = \frac{3 \times 10^{-3}}{n_{\mathrm{eff}}^{\mathrm{even}} - n_{\mathrm{eff}}^{\mathrm{odd}}}(m), \tag{9}$$

where $n_{\mathrm{eff}}^{\mathrm{even}}$ is the odd mode, $n_{\mathrm{eff}}^{\mathrm{odd}}$ is the even mode, and $\lambda$ is the wavelength. Figure 14 shows the walk-off lengths of the HE and EH modes at 1.55 $\mu$m.

The walk-off lengths of the HE and EH modes do not exhibit a regular increasing and decreasing trend. The maximum walk-off lengths of 89,909.38 m for the HE mode and 20,132.88 m for the EH mode indicate that a large walk-off length allows for better transmission distances.

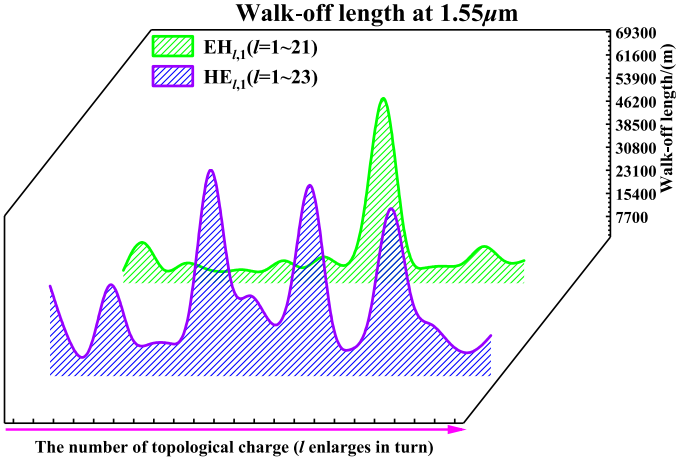


Fig. 14. (Color online) Walk-off length of the HE and EH modes at 1.55 $\mu$m.

Table 3. Comparison of OAM mode performance with other paper.

| Refs. | Dispersion ps/(km · nm) | OAM Purity | Nonlinear Coefficient ($km^{-1} \cdot W^{-1}$) | Confinement loss (dB/m) |
|---|---|---|---|---|
| 21 | 53.01 | — | 0.48 | $10^{-12}$–$10^{-10}$ |
| 22 | — | 0.98 | 0.36–0.70 | $10^{-12}$–$10^{-7}$ |
| 34 | $>50.00$ | — | 1.10–1.75 | $<10^{-8}$ |
| 44 | 31.80 | 0.99 | 1.40 | $10^{-10}$–$10^{-8}$ |
| This work | 38.03 | 0.99 | 0.34 | $10^{-10}$–$10^{-8}$ |

### 3.9. *Comparison of performance with existing literature*

After a series of optimizations, by comparing Table 3 with existing literature on dispersion, mode purity, nonlinear coefficient, and limiting loss, it is concluded that the proposed ARF model has higher mode purity and smaller nonlinear coefficient. Although the dispersion is slightly higher and the loss is slightly greater compared to Refs. 21 and 44, it still has good characteristics for transmitting OAM modes within a reasonable range. Therefore, this work improves the quality of information transmission in large capacity optical fiber communication, and provides a new idea for the development of orbital angular momentum in the future.

## 4. Conclusion

An ARF that can transmit 86 OAM modes stably in the wavelength range between 1.2 $\mu$m and 2.0 $\mu$m is designed and analyzed. Theoretical assessment shows that the effective refractive index differences are greater than $1 \times 10^{-4}$ and there is low mode simplicity. This structure has low and flat dispersions of only 38.03 ps/(km-nm) and 4.81 ps/(km-nm) for the $HE_{1,1}$ mode. The limiting loss is very low at a wavelength of 1.55 $\mu$m being between $10^{-10}$–$10^{-8}$ dB/m, thereby allowing stable transmission. The fiber has a maximum effective mode field area of 154.70 $\mu m^2$ at 1.55 $\mu$m and can carry more photon energy. It has a small nonlinear coefficient of 0.44 $km^{-1} \cdot W^{-1}$, which is favorable to OAM mode transmission. Moreover, the mode purity of all OAMs is above 96.17%, and the maximum NA is 0.9189 resulting in increased transmission efficiency. The anti-resonance fiber has many potential applications in fiber optics communication.

## Acknowledgments

This work was jointly supported by the Heilongjiang Provincial Natural Science Foundation of China [JQ2023F001], the Outstanding Young and Middle-aged Research and Innovation Team of Northeast Petroleum University [KYCXTD201801], Local Universities Reformation and Development Personnel Training Supporting Project from Central Authorities, Postdoctoral Scientific Research Development Fund of Heilongjiang Province (LBH-Q20081), City University of Hong Kong

Donation Research Grant [DON-RMG No. 9229021], City University of Hong Kong Strategic Research Grant [SRG 7005505], and City University of Hong Kong Donation Grant [9220061].

## References

1. S. Kumar and M. J. Deen, *Fiber Optic Communications: Fundamentals and Applications* (John Wiley & Sons, New Jersey, 2014).
2. Y. Zheng, Z. Yi, L. Liu, X. Wu, H. Liu, G. Li, L. Zeng, H. Li and P. Wu, *Appl. Therm. Eng.* **230** (2023) 120841.
3. S. Liang, F. Xu, W. Li, W. Yang, S. Cheng, H. Yang, J. Chen, Z. Yi and P. Jiang, *Appl. Therm. Eng.* **232** (2023) 121074.
4. Z. Chen, P. Cai, Q. Wen, H. Chen, Y. Tang, Z. Yi, K. Wei, G. Li, B. Tang and Y. Yi, *Electronics* **12**(12) (2023) 2655.
5. F. Wu, P. Shi, Z. Yi, H. Li and Y. Yi, *Micromachines* **14**(5) (2023) 985.
6. R. Lai, P. Shi, Z. Yi, H. Li and Y. Yi, *Micromachines* **14**(5) (2023) 953.
7. F. Qin, J. Chen, J. Liu, L. Liu, C. Tang, B. Tang, G. Li, L. Zeng, H. Li and Z. Yi, *Sol. Energy* **262** (2023) 111796.
8. B. Mukherjee, *IEEE. J. Sel. Areas Commun.* **18**(10) (2000) 1810.
9. D. M. Spirit, A. D. Ellis and P. E. Barnsley, *IEEE Commun. Mag.* **32**(12) (1994) 56.
10. Z.-M. Qiu and Y. Wong, *Comput. Ind.* **58**(5) (2007) 453.
11. H. Ishio, J. Minowa and K. Nosu, *J. Light. Technol.* **2**(4) (1984) 448.
12. N. Bozinovic, Y. Yue, Y. Ren, M. Tur, P. Kristensen, H. Huang, A. E. Willner and S. Ramachandran, *Science* **340**(6140) (2013) 1545.
13. G. Li, N. Bai, N. Zhao and C. Xia, *Adv. Opt. Photonics* **6**(4) (2014) 413.
14. A. Jesacher, S. Fürhapter, S. Bernet and M. Ritsch-Marte, *Phys. Rev. Lett.* **94**(23) (2005) 233902.
15. K. Kikuchi, *J. Light. Technol.* **34**(1) (2015) 157.
16. Q. Wu, Y. Semenova, B. Yan, Y. Ma, P. Wang, C. Yu and G. Farrell, *Opt. Lett.* **36**(12) (2011) 2197.
17. N. Borhani, E. Kakkava, C. Moser and D. Psaltis, *Optica* **5**(8) (2018) 960.
18. W. Liu, C. Hu, L. Zhou, Z. Yi, C. Liu, J. Lv, L. Yang and P. K. Chu, *Physica E Low Dimens. Syst. Nanostruct.* **138** (2022) 115106.
19. C. Liu, J. Lü, W. Liu, F. Wang and P. K. Chu, *Chin. Opt. Lett.* **19**(10) (2021) 102202.
20. Y. Yue, L. Zhang, Y. Yan, N. Ahmed, J. Y. Yang, H. Huang, Y. Ren, S. Dolinar, M. Tur and A. E. Willner, *Opt. Lett.* **37**(11) (2012) 889.
21. W. Huang, Y. You, B. B. Song and S. Y. Chen, *Optoelectron. Lett.* **16**(1) (2020) 34.
22. Q. Ma, A. Luo and W. Hong, *J. Light. Technol.* **39**(9) (2021) 2971.
23. L. Xu, C. Liu, H. Fu, J. Wang, X. Li, J. Lv, L. Yang and P. K. Chu, *Opt. Eng.* **61**(9) (2022) 096101.
24. H. Fu, Z. Yi, Y. Shi, C. Liu, J. Lv, L. Yang and P. K. Chu, *J. Mod. Opt.* **68**(15) (2021) 784.
25. J. Konečný, H. B. McMahan, F. X. Yu, P. Richtárik, A. T. Suresh and D. Bacon, preprint, arXiv:1610.05492 (2016).
26. M. M. Hassan, L. F. Abdulrazak, A. G. Alharbi, K. Ahmed, F. M. Bui, F. A. Al-Zahrani and M. S. Uddin, *Alex. Eng. J.* **61**(12) (2022) 9891.
27. X. Chen, X. Hu, L. Yang, J. Peng, H. Li, N. Dai and J. Li, *Opt. Express* **27**(14) (2019) 19548.
28. S. Chaudhuri, L. D. Van Putten, F. Poletti and P. J. Sazio, *J. Light. Technol.* **34**(18) (2016) 4228.

29. H. Fu, C. Liu, C. Hu, L. Zhou, Y. Shi, J. Lv, L. Yang and P. K. Chu, *Opt. Eng.* **60**(7) (2021) 076102.
30. K. Liu, H. Liu, Y. Qin, Y. Cheng, S. Wang, X. Li and H. Wang, *IEEE. Trans. Antennas Propag.* **64**(9) (2016) 3850.
31. H. Fu, M. Zhu, C. Liu, Z. Yi, J. Lv, L. Yang, F. Wang, Q. Liu, W. Su, X. Li and P. K. Chu, *Opt. Eng.* **61**(2) (2022) 026111.
32. H. Fu, C. Liu, Z. Yi, X. Song, X. Li, Y. Zeng, J. Wang, J. Lv, L. Yang and P. K. Chu, *J. Opt.* **52**(1) (2023) 307.
33. C. Brunet, P. Vaity, Y. Messaddeq, S. LaRochelle and L. A. Rusch, *Opt. Express* **22**(21) (2014) 26117.
34. W. Wang, C. Sun, N. Wang and H. Jia, *Opt. Commun.* **471** (2020) 125823.
35. S. Qiu, J. Yuan, X. Zhou, F. Li, Q. Wang, Y. Qu, B. Yan, Q. Wu, K. Wang, X. Sang, K. Long and C. Yu, *Sensors* **20**(22) (2020) 6539.
36. J. Yang, H. Zhang, X. Zhang, Z. Chen, L. Xi and W. Zhang, *Opt. Fiber Technol.* **64** (2021) 102543.
37. E. Liu, W. Tan, B. Yan, J. Xie, R. Ge and J. Liu, *J. Phys. D* **52**(32) (2019) 325110.
38. S. Chen, Z. Xie, H. Ye, X. Wang, Z. Guo, Y. He, Y. Li, X. Xuan and D. Fan, *Light Sci. Appl.* **10**(1) (2021) 222.
39. G. Yilmaz and S. E. Karlik, *Sens. Actuator A Phys.* **125**(2) (2006) 148.
40. M. M. Hassan, M. A. Kabir, M. N. Hossain, B. Biswas, B. K. Paul, and K. Ahmed, *Opt. Quantum Electron.* **52**(1) (2020) 8.
41. M. Xu, G. Zhou, C. Chen, G. Zhou, Z. Sheng, Z. Hou and C. Xia, *J. Opt.* **47** (2018) 428.
42. C. Liu, H. Fu, Y. Lv, Z. Yi, J. Lin, J. Lv, L. Yang and P. K. Chu, *Optik* **265** (2022) 169471.
43. M. F. Israk, M. A. Razzak, K. Ahmed, M. M. Hassan, M. A. Kabir, M. N. Hossain, B. K. Paul and V. Dhasarathan, *Opt. Commun.* **473** (2020) 126003.
44. Y. Lei, X. Xu, N. Wang and H. Jia, *J. Opt.* **20**(10) (2018) 105701.
45. D. Vigneswaran, M. S. M. Rajan, B. Biswas, A. Grover, K. Ahmed and B. K. Paul, *Opt. Quantum Electron.* **53** (2021) 1.
46. I. D. Rukhlenko, M. Premaratne and G. P. Agrawal ,*Opt. Lett.* **37**(12) (2012) 2295.
47. F. A. Al-Zahrani and M. M. Hassan, *Alex. Eng. J.* **60**(6) (2021) 5065.
48. S. H. Huang, Q. C. Ma, W. C. Chen, H. Z. Liu, X. B. Xing, H. Cui, Z. C. Luo, W. C. Xu and A. P. Luo, *Appl. Phys. B LASERS O* **125** (2019) 1.
49. G. P. Agrawal, *Nonlinear Science at the Dawn of the 21st Century* (Springer, New York, 2000), pp. 195–211.
50. S. Kumar and D. Yang, *Opt. Lett.* **36**(7) (2011) 1038.
51. H. Zhang, W. Zhang, L. Xi, X. Tang, X. Zhang and X. Zhang, *IEEE Photon. Technol. Lett.* **28**(13) (2016) 1426.
52. X. Jin, B. A. Hristovski, C. M. Collier, S. Geoffroy-Gagnon, B. Born and J. F. Holzman, in *Optical Components and Materials*, Vol. XIII 9744 (SPIE, 2016), p. 60.
53. B. Biswas, K. Ahmed, B. K. Paul, M. A. Khalek and M. S. Uddin, *Results Phys.* **13** (2019) 102184.
54. M. S. Islam, J. Sultana, K. Ahmed, M. R. Islam, A. Dinovitser, B. W. H. Ng and D. Abbott, *IEEE Sens. J.* **18**(2) (2017) 575.
55. Y. Koike and K. Koike, *J. Polym. Sci. B Polym. Phys.* **49**(1) (2011) 2.
56. W. Liu, Y. Shi, Z. Yi, C. Liu, F. Wang, X. Li, J. Lv, L. Yang and P. K. Chu, *Opt. Express* **29**(25) (2021) 40734.
57. W. Liu, C. Hu, L. Zhou, Z. Yi, Y. Shi, C. Liu, J. Lv, L. Yang and P. K. Chu, *Mod. Phys. Lett. B* **36**(01) (2022) 2150499.

58. Y. Jiang, G. Ren, H. Li, M. Tang, Y. Liu, Y. Wu, W. Jian and S. Jian, *Appl. Opt.* **56**(7) (2017) 1990.
59. F. A. Al-Zahrani and K. Ahmed, *Alex. Eng. J.* **59**(6) (2020) 4889.
60. Y. Wang, Y. Lu, C. Bao, W. Geng, Y. Fang, B. Mao, Z. Wang, Y. Z. Liu, H. Huang, Y. Ren, Z. Pan and Y. Yue, *IEEE Access* **9** (2021) 66999.
61. W. Liu, C. Liu, J. Wang, J. Lv, Y. Lv, L. Yang, N. An, Z. Yi, Q. Liu, C. Hu and P. K. Chu, *Results Phys.* **47** (2023) 106365.